Available online at www.sciencedirect.com

ScienceDirect

International Journal of Solids and Structures 45 (2008) 921–942

INTERNATIONAL JOURNAL OF SOLIDS AND STRUCTURES

www.elsevier.com/locate/ijsolstr

Cathode edge displacement by voiding coupled with grain boundary grooving in bamboo like metallic interconnects by surface drift-diffusion under the capillary and electromigration forces

Tarik Omer Ogurtani *, Oncu Akyildiz

Department of Metallurgical and Materials Engineering, Middle East Technical University, 06531 Ankara, Turkey

Received 24 May 2006; received in revised form 14 May 2007
Available online 19 September 2007

Abstract

The kinetics of cathode edge shrinkage and displacement (drift) coupled strongly with the grain boundary (GB) grooving is investigated using the novel mathematical model developed by Ogurtani, in sandwich type thin film bamboo lines. The computer simulations are performed under the constant current (CC) and the switch-over constant voltage (SOCV) operations. The cathode drift velocity and the cathode failure time show the existence of two distinct phases, depending upon the normalized electron wind intensity parameter χ; the capillary ($\chi \leqslant 0.01$) and the electromigration (EM) dominating regimes ($\chi > 0.01$), having current exponent n, equal to 0 and 1, respectively. Analysis of various experimental data on the cathode drift velocity results a consistent value for the surface drift-diffusion coefficient, $1.0 \times 10^{-5} \exp(-1.00\ \mathrm{eV}/kT)\ \mathrm{m}^2\ \mathrm{s}^{-1}$, for copper interconnects exposed to some contaminations during the processing and testing stages. This is found to be an excellent agreement with the experimental values reported in the literature after applying the proper $1/kT$ correction on the apparent activation enthalpy associated with Nernst–Einstein mobility relationship. The complete cathode failure time (CCFT) due to the cathode area shrinkage by voiding is also formulated by inverse scaling and normalization procedures, which show exactly the same capillary and EM dominating regimes. This formula can be used to predict very accurate CCFT for metallic lines with bamboo-like, near-bamboo, and even with polycrystalline structures by proper calculation of the cathode-edge path length (CEPL) parameter, in terms of the actual line width, the thickness and the grain size.

Keywords: Computer simulations; Models of non-equilibrium phenomena; Surface diffusion; Surface morphology; Electromigration; Grain boundary grooving; Cathode drift

1. Introduction

The dynamical phenomena studied in materials science are often too complex to be reduced to moving and free boundary value problems in terms of integro-differential equations through proper boundary conditions

* Corresponding author. Tel.: +90 312 210 2512; fax: +90 312 210 1267.
E-mail addresses: ogurtani@metu.edu.tr (T.O. Ogurtani), e109641@metu.edu.tr (O. Akyildiz).

0020-7683/$ - see front matter
doi:10.1016/j.ijsolstr.2007.09.007

that represent the realistic interactions with the surrounding media. Only in some special cases (Ogurtani et al., 2003) there is an elegant mathematical description, supplemented by proper numerical methods, allowing us to direct quantitative comparison with experimental observations. So many years, the subject of capillary-driven morphological evolution of surfaces and interfaces in condensed matter, continues to be a challenging theoretical problem in materials science, especially under the action of applied force fields (e.g. electrostatic and thermo-mechanical stress systems), without having any serious robust non-equilibrium thermodynamics or statistical mechanics treatments. This awkward situation has started to change recently (Ogurtani and Oren, 2005) since the sub-microscopic nature of the electronic devices has pushed the surfaces and interfaces onto the front lines as the primary agents in the determination of catastrophic failure of interconnects used in the microelectronic industry.

Recently, the technology transition from conventional Al/oxide interconnects to dual-damascene Cu/low-k interconnects has increased the concerns about long-term EM reliability. It has been observed (Hu et al., 2002) that the EM life time is mostly dependent on the atomic transport at the Cu/SiNx interface and/or the Cu/Ta liner interface as claimed by some researches (Liniger et al., 2002) not on the intrinsic character of the Cu lattice or atomic transport at grain boundaries. Also it has been shown that (Hu et al., 2004; Lloyd et al., 2005) 10–20 nm thick metal caps (CoWP, CoSnP, or Pd) significantly improve the EM lifetime. This is just opposite to the case in the well studied Al(Cu) system. In fact, the EM mechanism leading to failure in Cu is a controversial topic as many studies conducted with various testing methods have produced wide-ranging activation energies, implying that the dominant failure mechanism is highly dependent on sample configuration and the test methods. Nevertheless, in near-bamboo and bamboo structures, the activation energies for oxides, porous MSQs (methylsilsesquioxane), and organic polymer dielectrics were found to be in the range of 0.8–1.0 eV, suggesting that the mass transport is dominated by interfacial drift diffusion at the Cu and SiN_x cap-layer interface regardless of the dielectric materials (Lee and Ho, 2004). Similarly, Liniger et al. (2002) suggested that grain thinning or edge displacement mechanisms are responsible for the cathode void growth, and the surface drift-diffusion paths are the primary agents for the necessary mass transport, in their in situ studies on the void growth kinetics in unpassivated Cu damascene lines with TaN/Ta liner.

These observations have motivated us to perform a through study of the sidewalls (i.e., upper and/or lower surfaces) and cathode edge drift-diffusion problem as semi-connected interfacial system via computer simulations by utilizing more realistic free and moving boundary conditions (FM-BC) at the cathode edge. This article primarily focuses on the non-equilibrium thermodynamic treatment of the cathode shrinkage and drift processes coupled with the GB grooving, and carried out Blech-type experimental configuration, under CC as a further supplement for our previous work (Ogurtani and Akyildiz, 2005). In that work the main concern was the study of the morphological surface evolution dynamics associated with GB grooving kinetics coupled with the cathode contact area shrinkage and/or cathode voiding using SOCV operation.

A full account for the micro-electronic applications of Ogurtani theory (2006) on the triple junction (TJ) and ordinary points is reported recently in connection with the computer simulation studies on the effect of EM induced void GB interactions in the determination of cathode-pad failure time (CPTF) for copper and aluminum (Ogurtani and Oren, 2004, 2005) interconnects with bamboo and near-bamboo structures. These studies have furnished extremely rich and sound analytical expressions to extrapolate accelerated test results down to the device operation conditions, in addition to the extraction of the drift-diffusion coefficients related to both the clean and contaminated surfaces from published experimental data.

2. Physical and mathematical modeling

The evolution kinetics of surfaces or interfacial layers (simply or multiply connected domains) may be described by the following well-posed moving boundary value problem (BVP) in two dimensional (2D) space, respectively for ordinary points and TJ singularities, in terms of normalized and scaled parameters and variables. In these formulas the surface drift-diffusion, which may be represented by an angular dependent post factor, $D''(\theta,\phi)$, has been taken as anisotropic, on the contrary, for the time being the specific Gibbs free energy of the interfacial layer has been assumed to be isotropic. The generalization of this irreversible thermodynamic theory to 3D space, by taking into account not only the anisotropy in the surface drift-diffusion but also the anisotropy in the surface Gibbs specific free energy, is also deduced by Ogurtani, while he was revising

the manuscript published in IJSS (Ogurtani and Oren, 2005) in order to show its universality. The full account of 3D theory will be published elsewhere. The surface displacement velocity denoted by $\overline{V}_{\rm ord}$ at the ordinary points is given by the following governing equation in the normalized and scaled space:

$$\overline{V}_{\rm ord} = \frac{\partial}{\partial \bar{\ell}}\left[D''(\theta,\phi)\frac{\partial}{\partial \bar{\ell}}(\Delta \bar{g}_{\rm vb} + \chi\bar{\vartheta} + \bar{\kappa})\right] - \overline{M}_{\rm vb}(\Delta \bar{g}_{\rm vb} + \bar{\kappa}), \tag{1}$$

where $\bar{\kappa}$ is the local curvature and is taken to be positive for a convex void or a concave solid surface, $\bar{\ell}$ is the curvilinear coordinate along the void surface (arc length). $\Delta\bar{g}_{\rm vb} = (\bar{g}_{\rm v} - \bar{g}_{\rm b})$ denotes the normalized volumetric Gibbs free energy density difference between the realistic void phase (vapor) and the bulk matrix, and it is normalized with respect to the specific surface Gibbs free energy of the void denoted by g_σ. χ is the electron wind intensity parameter, $\bar{\vartheta}$ is the normalized electrostatic potential generated at the surface layer due to the applied electric field intensity. In Eq. (1), the bar sign over the letters indicates the following scaled and normalized quantities:

$$\bar{t} = t/\tau_0, \quad \bar{\ell} = \ell/\ell_0, \quad \bar{\kappa} = \kappa\ell_0, \quad \bar{w}_0 = w_0/\ell_0, \quad \overline{L} = L/\ell_0 \tag{2}$$

$$\Delta\bar{g}_{\rm vb} = \frac{\breve{g}_{\rm vb} r_0}{g_\sigma}, \quad \bar{\vartheta} = \vartheta/(E_0\ell_0), \quad \chi = e|\widehat{Z}|E_0\ell_0^2/(\Omega_\sigma g_\sigma). \tag{3}$$

The time and space variables $\{t,\ell\}$ have been scaled in the following fashion: First of all, $\widehat{M}_\sigma$, an atomic mobility associated with mass flow at the surface layer, is defined by the relationship given $\widehat{M}_\sigma = [D_\sigma h_\sigma/kT\Omega_\sigma]$, where D_σ is the surface diffusion coefficient, h_σ is the thickness of the surface layer, Ω_σ is the atomic mean volume, and kT has the usual meaning. Then a new time scale is introduced by $\tau_0 = \ell_0^4/(\Omega_\sigma^2\widehat{M}_\sigma g_\sigma)$, where ℓ_0 is the arbitrary length scale which is for the present simulation studies chosen as $\ell_0 = 2w_0/3$, where w_0 is the half width of the interconnect and L and $h_{\rm s}$ are the specimen length, and height, respectively.

In these equations, E_0 denotes the electric field intensity directed along the specimen longitudinal axis. $e|\widehat{Z}|$ is the effective charge, which may be given in terms of atomic fractions, x^i, by $\widehat{Z} = \sum_i x^i\widehat{Z}^i$ for multi-component alloys. The generalized mobility, $\widehat{M}_{\rm vb}$, associated with interfacial displacement reaction taking place during the surface growth process (adsorption or desorption) is also normalized and given by

$$\overline{M}_{\rm vb} = \frac{\widehat{M}_{\rm vb}\ell_0^2}{\widehat{M}_\sigma}. \tag{4}$$

TJ drift velocity along the rigid GB can be represented by

$$\overline{V}_{\rm g}^{\rm long} = \overline{M}^{\rm long}\frac{\overline{\Omega}_{\rm g}\bar{d}_{\rm a}}{2\overline{\Omega}_\sigma^2\bar{h}_{\rm g}}[2\lambda - (\cos\theta^+ + \cos\theta^-)], \tag{5}$$

where $\bar{d}_{\rm a}$, and $\bar{h}_{\rm g}$ are the interatomic distance and the thickness of the grain boundary layer, respectively. $\overline{\Omega}_{\rm g}$ and $\overline{\Omega}_\sigma$ are the mean atomic volumes of chemical species, respectively, in the GB and the void surface layer. The superscripts plus and minus over the dihedral angles θ^+ and θ^-, respectively, indicate the right and left faces of the GB-groove. $\overline{M}^{\rm long}$ is the longitudinal generalized mobility of TJ, which is defined below. λ is the wetting parameter associated with TJ, which is assumed to be isotropic in the present case study. It may be given by $\lambda = g_{\rm g}/2g_\sigma$, where $g_{\rm g}$ and g_σ are the specific surface Gibbs free energy densities associated, respectively, with the grain boundary and void surface layers.

The following boundary conditions at the TJ in terms of right and left side fluxes may be written as

$$\overline{J}_0^{\mp} = \mp\overline{M}^{\rm long}\frac{\bar{d}_{\rm a}}{2\overline{\Omega}_\sigma^2}(\lambda - \cos\theta^{\mp}) \mp \overline{J}_{\rm g}/2 + \overline{J}_{\vartheta}^{+}\overline{M}^{\rm trans}\frac{\bar{d}_{\rm a}}{\overline{\Omega}_\sigma^2}(\sin\theta^+ - \sin\theta^-). \tag{6}$$

This particular partition of the incoming grain boundary flux $\overline{J}_{\rm g}$ between $\overline{J}_0^+$ and $\overline{J}_0^-$ is a matter of convenience, otherwise it is completely arbitrary as long as one satisfies the generalized law of conservation of particles including the phase transformation at the TJ, which is given by $\overline{J}_0^- + \overline{J}_{\rm g} - \overline{J}_0^+ + \bar{h}_{\rm g}\overline{\Omega}_{\rm g}^{-1}\overline{V}_{\rm g}^{\rm long} = 0$. $\overline{J}_{\rm g}$ denotes the normalized atomic fluxes associated with grain boundary mass flow due to some driving force such

as thermal stress field inhomogeneities, and the drift-diffusion due to EM. The latter flux contribution is given by $\overline{J}_{\mathrm{gb},\vartheta} = -\overline{M}_{\mathrm{gb}}\chi(\hat{n}_{\mathrm{g}} \cdot \operatorname{grad}\bar{\vartheta})/\overline{\Omega}_{\mathrm{g}}$, where $\hat{n}_{\mathrm{g}}$ is the orientation of the grain boundary and $\overline{M}_{\mathrm{gb}}$ is the normalized grain boundary diffusion mobility. $\overline{J}_{\vartheta}$ is the usual contribution due to EM acting on both branches of the void at the TJ. The electrostatic potential exhibits a well-known discontinuity at the TJ (at sharp edges and corners, etc.). On the contrary to this behavior, the tangential component of the electric field intensity vector along the interfacial layers or surfaces is continuous everywhere including the TJ singularity. In the present problem, the positive direction of the flux is chosen as the clock-wise direction around the interconnect body starting from the upper left edge (anode side).

In the earlier relationships, the following scaled and normalized quantities were also employed. $\overline{M}^{\mathrm{trans}}$ corresponds to the normalized transverse mobility of the TJ with respect to the mobility of the surface diffusion denoted by $\widehat{M}_{\sigma}$. The explicit expressions may be given by

$$\widehat{M}^{\mathrm{long}} = \frac{\mathfrak{R}^{\mathrm{long}}}{kT}\frac{h_{\mathrm{g}}}{\Omega_{\mathrm{g}}}, \quad \widehat{M}^{\mathrm{trans}} = \frac{\mathfrak{R}^{\mathrm{trans}}}{kT}\frac{h_{\sigma}}{\Omega_{\sigma}}, \quad \widehat{M}_{\mathrm{gb}} = \frac{D_{\mathrm{g}}}{kT}\frac{h_{\mathrm{g}}}{\Omega_{\mathrm{g}}}, \quad \widehat{M}_{\sigma} = \frac{D_{\sigma}}{kT}\frac{h_{\sigma}}{\Omega_{\sigma}} \tag{7}$$

where $\mathfrak{R}^{\mathrm{long}}$ and $\mathfrak{R}^{\mathrm{trans}}$ are the transition rates associated with the longitudinal and transverse displacements of the TJ, which may be calculated by Yeremin (1979) transition rate theory. D_{g} is grain boundary diffusion coefficient. In the formulation of the problem, we have adapted the convention such that the positive direction of motion is always towards the bulk material whether one deals with inner voids or outer surfaces or interfaces.

For the boundary element method (BEM) applications, the size of the scaling length becomes important for the stress calculations to obtain proper convergence, which utilizes the Lord Kelvin's solution for the elastostatic problems (Lord Kelvin and Tait, 1789). The surface specific Gibbs free energy, g_{σ}, plays a very important role in the earlier definitions. $\Delta\bar{g}_{\mathrm{vb}}(\Delta\bar{g}_{\mathrm{vb}} < 0$ evaporation or void growth) is the volumetric Gibbs free energy difference (the Gibbs free energy of transformation, GFEDoT) between the realistic void and the bulk phase, and it is normalized with respect to the specific surface Gibbs free energy.

3. Computer simulation results

In our present computer simulation studies, it is assumed that the sample is sandwiched between top and bottom high resistance ($TiAl_3$, TiN, etc.) coatings, which constitute diffusion barrier layers together with the substrate. It is also assumed here that only the sidewalls and the edges of the interconnect line are subjected to the surface drift-diffusion, and they are exposed to an environment whose conductivity is neglected in this study. In certain cases (Hu et al., 2001) in which the upper and lower interfaces of the interconnect line become predominant paths for the drift-diffusion, the results of our computer simulation may still be applied rigorously by replacing the line width parameter, w, with the line thickness denoted by h. In some cases (Liniger et al., 2002), the unpassivated upper surface becomes the dominant diffusion path and the lower interface stays inactive (insulating boundary), then w should be replaced by $2h$ due to the reflection symmetry of the solutions of the present sample configuration with respect to the longitudinal mid-plane, which acts implicitly as an insulating boundary. In the evaluation of the electromigration life time of a Cu damascene interconnect by the cathode edge displacement or contact-area shrinkage via voiding, during which the effective electrical contact area is primarily fixed by the fractional uncovered cross section of the vias, one may employ the results of the present computer simulations even without any modification. However, one should only pay attention to usage of geometric information in the calculation of the effective path length denoted by $\hat{w}$. Especially in the case of concurrent drift-diffusion processes operating along the multiple paths in the interconnect line, it is vital to use the ad hoc expression mostly employed in reaction kinetics to evaluate the effective path, which directly enters in our formulas. These points will be further elaborated later in this paper by giving thorough analysis of some specific experiments published in the literature.

3.1. Cathode drift due to the EM induced voiding

The cathode drift experiments were performed on the samples having same configurations as described above. In the present simulation studies, it is assumed that the specimen have direct mechanical contact with

the electrodes (DMCE) at the cathode and anode edges in addition to the shunt action of the underlying substrate or vias in the case of Cu damascene interconnect configuration. In our numerical simulation technique it is completely immaterial how to impose the electrostatic field to the specimen in order to sustain a constant current application. Two different experimental procedures were applied to reveal this peculiar phenomenon. The first procedure as described in the previous article (Ogurtani and Akyildiz, 2005) uses reflecting boundary conditions (R-BC) at both ends of the interconnect specimen, and starts with application of the constant voltage differential to the electrodes up to the point where the almost complete cathode failure (95%) occurs by voiding. Under the constant voltage differential testing, the complete cathode detachment actually never takes place ($t_{CFT} \to \infty$), because of the exponential character of the phenomenon in the asymptotic region. Therefore, an external agent should activate the constant current source program as soon as the distance between the two leading nodes of the cathode edge becomes equal to the minimum segment length generated during the simulation experiments. This roughly corresponds to 5% of the total width in our discretization scheme.

The second approach employs FM-BC at the cathode edge and R-BC for the anode edge. The constant current source (CCS) may be put into the operation from the beginning of the simulation experiments rather than waiting for the end of the complete cathode failure by the shrinkage of the contact area, since the elapsed time for the cathode shrinkage by voiding (CSV) becomes finite and the switch over to the cathode tip displacement (drift) takes place naturally.

3.2. Switch-over constant voltage experiments, CV

In Fig. 1, a typical cathode shrinkage by voiding and the subsequent cathode drift by edge-displacement are plotted as a function of normalized time for two extreme cases, (a)$\chi = 0.01$ and (c) $\chi = 50$, where the interconnect thin metallic film is subjected to the mixed electrostatic boundary conditions as described above where, the cathode shrinkage is represented by the temporal or the instantaneous width of the contact area between interconnect line and the flat face of the cathode electrode. Similarly, the cathode edge-tip position of the interconnect line during the drift motion is measured by the distance between the cathode edge of the interconnect line and the face of the cathode electrode along the longitudinal symmetry axis of the specimen, after the

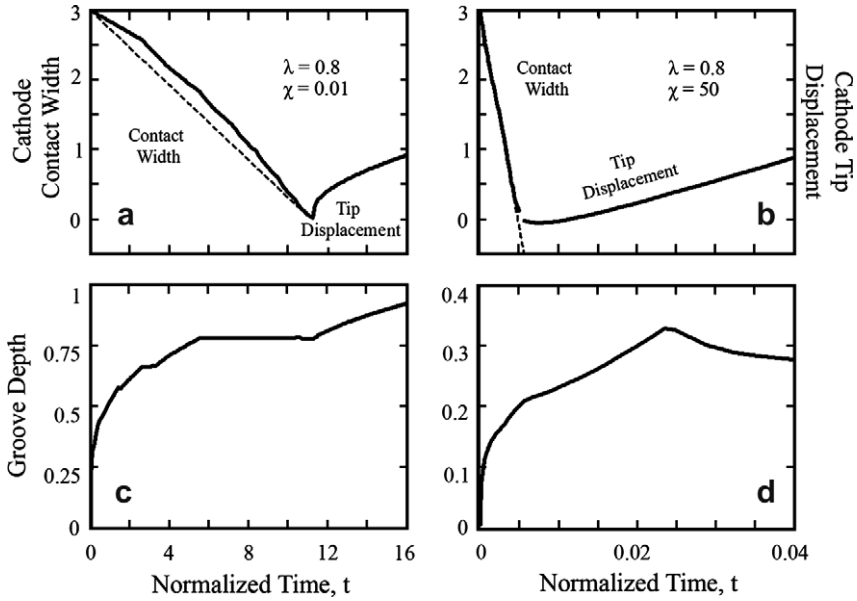

Fig. 1. The normalized instantaneous values of the cathode contact area, the cathode edge-tip displacement, and the concurrent groove penetration depths obtained from the SOCV simulations for two extreme cases, (a) and (b) for $\chi = 0.01$ and (c) and (d) for $\chi = 50$, are plotted versus normalized time. The distinct kinematics behavior of the capillary and the EM dominating regimes are clearly seen in these plots where the normalized length scale is used, which is given by $\ell_0 = 2w_0/3$.

contact between them completely breaks down. There is a knee on the groove depth profile, which is strongly correlated with the cathode-edge drift initiation process, which may be called as the end of the incubation period. The peaking in the groove profile is due to the groove displacement velocity inversion, and it is caused by the current crowding at the grain boundary TJ regions due to necking. In our simulation studies the groove penetration depth is computed, which measures the relative height of GB-groove tip with respect to the original flat surface of the interconnect line. According to the Mullins' classical small slope theory (Mullins, 1957), it is given by $h_{GB}(\bar{t}) = -0.7801745 \times [\lambda/\sqrt{1-\lambda^2}]\bar{t}^{0.25}$ in the normalized and scaled length and time domain employed in this paper.

This figure clearly shows the linear behavior of the cathode-drift phenomenon in the EM dominating regime (coinciding dashed line), but not in the capillary region where the parabolic variation with respect to time prevails. The slopes (drift velocity) of these drift-displacement time plots in the steady states show very systematic correlation with the applied electron wind intensity parameter χ. This behavior is also observed for the constant current source program that will be described in the next section. These results are analyzed by linear regression procedure, which produced the following analytical expression:

$$\bar{d}^{CV}_{drift}(\chi,\bar{t}) = (0.661\chi + 0.126)\bar{t} \tag{8}$$

where, $\bar{d}^{CV}_{drift}$ is the normalized cathode drift-displacement and $\bar{t}$ is the normalized elapsed time for the cathode drift, which is referred to the onset of the cathode edge displacement stabilization regime, which coincides with the end of the incubation period. Due to the sudden change over from the constant voltage regime to the constant current condition, some fluctuations in the cathode edge position always take place. The extrapolation of this relationship to zero electron wind intensity parameter ($\chi \to 0$) implies that there should be a cathode-drift phenomenon, which correspond to the case where there is no applied electric field imposed on the sample, $\chi = 0$. In reality, our extensive computer simulation studies showed that one cannot have any cathode voiding and drifting in the absence of the applied electric field as long as if one uses the R-BC at the cathode edge. Similarly, no mass accumulation takes place at the anode edge if one uses R-BC. However, as we will see in the next section; FM-BC at the cathode edge result voiding and cathode drifting even in the absence of the applied electric field. According to our preliminary studies, the application of FM-BC at both cathode and anode edges, under the action of applied electric field through the underlying shunt, results extremely interesting surface morphological variance, which are superimposed on the translational motion of the body as a whole. This again proves the vital importance of realistic physico-chemical boundary conditions in computer simulations in materials science as much as the governing integro-differential equations in describing the underlying process properly.

Now, we can transform above findings into the real time and space domain by inverse scaling procedure, which results following very unique relationship composed of two terms having completely different origins, namely: the electromigration induced drift and the capillarity enforced shape displacement to reach global thermo-physical equilibrium configuration

$$d^{CV}_{drift}(\chi,t) = 1.983\frac{D_\sigma h_\sigma e Z_\sigma \rho_b j}{wkT}t + 3.4\frac{\Omega_\sigma D_\sigma h_\sigma g_\sigma}{w^3 kT}t \tag{9}$$

Similarly one may define a fictitious knee-current density, where these two contributions to the cathode drift velocity become equal. This fictitious knee-current density does not have any physical meaning in practice but nevertheless roughly describes the change over point or the knee point on the phase transition curve. This curve describes the transition path from EM dominating regime $\chi \geqslant 1$ to the capillarity influence regime $\chi \leqslant 0.01$ through a transition stage that covers a large span in the applied electron wind intensity parameter or in the current density scale as will be shown later. This behavior will be rigorously elaborated and clarified in the next section by the edge-displacement incubations time versus the electron wind intensity parameter plot obtained by the computer simulations under the constant current density applications. According to above definition the drift knee-current density may be given by the following expression, which is about equal to $j^{drift}_{Knee} \cong 1.510^{11}$ Am^{-2} for a cupper interconnect having a line width of $w = 0.1$ μm, and the both sidewalls are exposed to the surface drift diffusion

$$j_{\text{Knee}}^{\text{drift}} \cong 1.7\frac{\Omega_\sigma g_\sigma}{w^2 e Z_\sigma \rho_{\text{b}}} \qquad \text{(Drift knee current density)} \tag{10}$$

This current density as will be seen in discussion section is about one order of magnitude larger than the actual current density used in most accelerated test structures (Hu et al., 2002a,b; Liniger et al., 2002). As we mentioned previously, even though the knee current density does not have any practical usage since the transition regime covers a large span that is about two orders of magnitude in the applied current density spectrum, still might have some institutive importance, which may be more appreciated when the behavior of the cathode drift velocity with the applied electric field is examined. Because of this reason alone the present time device operation conditions are well above the upper bond of the capillarity plateau region which is observed in laboratory test environment. For the unpassivated copper interconnect lines having contaminated top free surfaces ($h_c = 0.3$ μm) or the sidewalls ($w = 0.1$ μm) acting as dominant diffusion paths, the onsets of the transition stage, which is the end of the plateau region that characterized the capillary dominating regime starts at $J_{\text{Cu}} \approx 2.5 \times 10^7$ Am^{-2} and $J_{\text{Cu}} = 8.8 \times 10^8$ Am^{-2}, respectively. The knee current density is an inverse quadratic function of the line width (or the line thickness), which gives some hint that the miniaturization or down scaling of microelectronic devices may put further strain on the reliability considerations unless one avoids those interfaces and surfaces having high interfacial specific Gibbs free energy, which is the most important design parameter in this respect. Since the critical current density also depends linearly on the specific (interfacial) surface Gibbs free energy of the interfacial layer between the interconnect material and its surrounding coatings, and inversely on the bulk resistivity, the reduction of the surface Gibbs free energy with alloying and/or selective impurity segregation becomes an important design criteria.

Similarly, the steady state cathode drift velocity by voiding may be calculated from Eq. (9), by taking its differential and adjusting the terms, which reads

$$V_{\text{drift}}^{\text{CV}} = 1.983\frac{D_\sigma h_\sigma e Z_\sigma \rho_{\text{b}}}{wkT}[j + j_{\text{Knee}}^{\text{drift}}] \quad \text{(steady state cathode drift velocity)} \tag{11}$$

The close inspection of the first term in above equation shows that there is a very close resemblance between the cathode drift velocity in EM influence regime and the steady state drift velocity of a circular void in an infinite and isotropic interconnect as calculated analytically by Ho (1970), namely

$$V_{\text{drift}}^{\text{Void}} = \frac{2}{r_0}\frac{D_\sigma h_\sigma e \widehat{Z} \rho j}{kT} \tag{12}$$

where r_0 is the radius of the internal void.

To give a clear idea on the effects of the boundary conditions adapted for the cathode as well as the anode edges; we include various snapshots taken from the zero field simulation experiments and plotted in Fig. 2. This figure clearly shows the existence of the voiding (shrinkage) as well as the cathode edge displacement (drift), because of the application of FM-BC at the cathode edge. On the contrary to the cathode edge, there is no observable variation in the anode edge of the surface profile, where we have employed R-BC. At the end of the simulation the bi-crystal sample breaching into two pieces, and then start to evolve continuous into two generalized cylindrical shape specimens in 3D space. This grain splitting is in complete accord with the finite elements analysis of Huang et al. (2000). According to their Fig. 8, the aspect ratio of our sample $\beta \cong 13$ corresponds to a critical thermal groove angle of 22°, which is much smaller than our complementary dihedral angle of $53° = \arcsin(\lambda)$. The piece on the right hand side, which has free boundary conditions turns into cylinder with perfect circular cross section. The left hand side piece, because of R-BC on the anode edge shows droplet shape configuration having 90° tilt angle at the contact surface. Here, we should mentioned that we have also developed a wetting boundary condition (or interactive-BC) for the electrode–interconnect contact area using the irreversible thermodynamic similar to the GB-TJ formulation. Where, we have found that the cathode area shrinkage or the ridge formation is solely controlled by the surface Gibbs free energies at triple junction, exactly analog to the classical wetting theory, unless one has strong anisotropy, where the torque term might dominate the surface free energies and causes the ridge formation (Min and Wong, 2006).

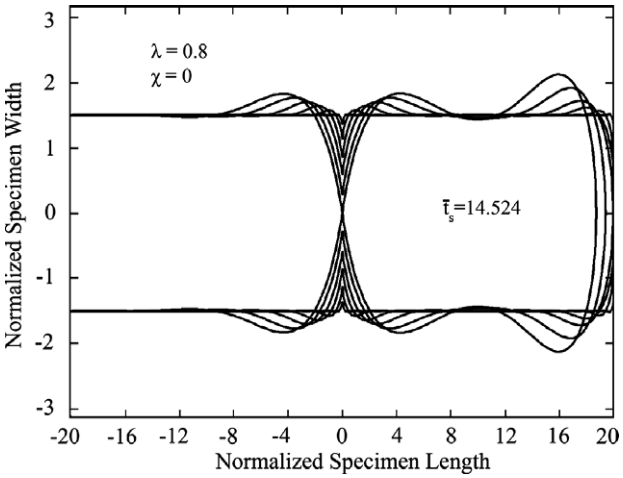

Fig. 2. Snapshots showing the surface morphological evolution and the cathode edge shrinkage and displacement of an interconnect bicrsytal metallic line under the capillary forces in the absence of the applied current. This computer simulation is performed using FM-BC at the cathode and R-BC at the anode edges on a sample having an aspect ratio of about $\beta = L/w_0 \simeq 13$. $\chi = 0$, the wetting parameter, $\lambda = 0.8$ (i.e. dihedral angle equal to $\theta^{\pm} = 37°$).

3.3. Constant current experiments, CC

The second approach employs FM-BC at the cathode edge and R-BC at the anode edge of the interconnect material having an aspect ratio of $\xi \cong 20$ from the beginning of the computer experiments. This way CC simulation may be put into operation from the beginning of the simulation experiments rather than waiting for the completion of the cathode failure by the shrinkage of the contact area. This can be easily accomplished by the decomposition of the complete solution of the electrostatic problem into particular and complementary parts relying on the principle of superposition associated with the linear partial differential equation (LPDE) rather than the direct boundary element method (BEM), which is mostly used by combining it with finite element methods (FEM) in the literature. In this proposed decomposition method, the indirect boundary element method (IBEM) will be used only for the complementary solution in order to satisfy the Neumann and/or Dirichlet boundary conditions. Since the particular solution should only have to satisfy the governing LPDE, one would have a great flexibility to select a proper functional form (i.e., any polynomial degree of $\{n-1\}$ in terms of the Cartesian coordinate representation in the solution of ∇^n operator to fit the experimental conditions and requirements).

First of all, as a particular solution of the Laplace operator ∇^2, we apply a constant and uniform external electric field ($\vec{E}_0 = \hat{i}E_0$) to the 2D space in which the sample is situated. Physically this can be realized if the under layer of high resistance material (Ta, TiN and $TiAl_3$) is acting as a shunt, similar to Blech's experiments (Blech and Kinsborn, 1975) or using vias as in case of Cu Damascene configuration. Then, during the calculation of the virtual charge distribution at the specimen boundaries (the sidewalls and the cathode and anode edges) by using IBEM for the complementary solution, we modified the Neumann boundary conditions (NBC) such that the part of the cathode end bounded by the original sidewalls (w-width) of the specimen and the whole anode edge should have zero virtual electric field intensity projection, not along the surface normal but along the direction of the applied field, regardless of their shapes. On the contrary to this restriction, at the sidewalls the induced electric field intensity should counter act against to normal component of the field generated by the particular solution at the boundary (usual NBC). Hence for the complete solution of BVP, the actual electric field intensity at the cathode and anode boundaries becomes equal to the applied electric field intensity, and the sidewalls become fully insulated against the current leakage.

In Fig. 3, the cathode-edge area shrinkage by voiding and the cathode drifting by edge displacement are presented for various electron wind intensities. We have also applied the linear regression analysis on the cathode voiding or shrinkage experiments, and obtained the following analytical expression for the normalized

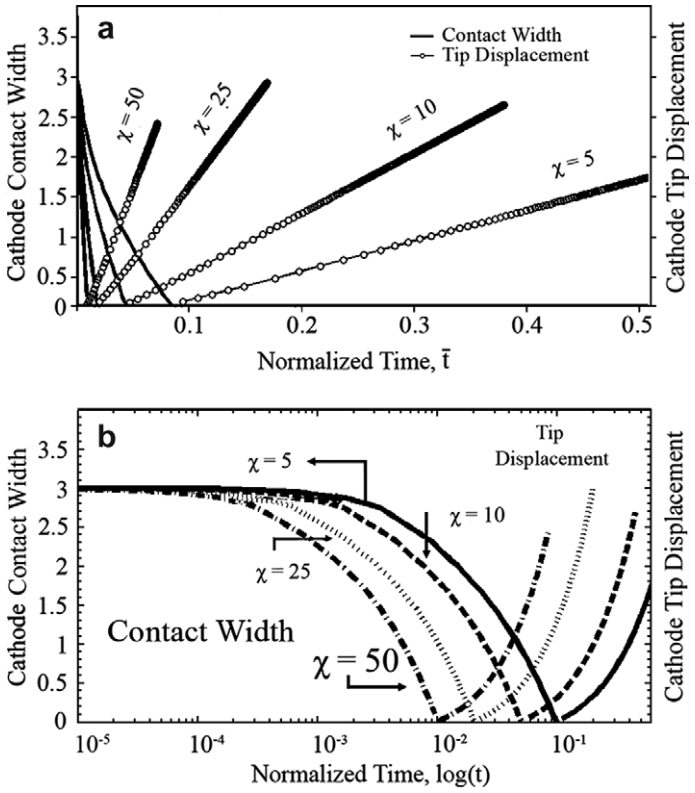

Fig. 3. The normalized instantaneous values of the cathode contact area (shrinkage), and the cathode edge-tip displacement (edge-drift) measured from the flat face of the cathode electrode, obtained from CC simulations, versus normalized time on (a) the linear and (b) the semi-logarithmic plots for various values of electron wind intensity parameter, χ where, the normalized length scale is used, which is given by $\ell_0 = 2w_0/3$.

cathode-edge area $\overline{A}^{\mathrm{CC}}(x,\bar{t})$ with respect to the initial cross section $A_0^{\mathrm{CC}} = hw$ or inverse electrical resistivity variations with respect the normalized time

$$\begin{aligned}\overline{A}^{\mathrm{CC}}(x,\bar{t}) \equiv \left[\frac{R}{R_0}\right]^{-1} &= \frac{2}{3}[1-4\chi\bar{t}]\times[1+0.5\exp(-10\chi\bar{t})] \\ &\cong [1-4\chi\bar{t}] \Rightarrow \equiv \left[1-\frac{3}{2}\frac{D_\sigma h_\sigma e Z_\sigma \rho_{\mathrm{b}} j}{w^2 kT}t\right]\end{aligned} \tag{13}$$

Here, one has the following relationship: $\chi\bar{t} \equiv (D_\sigma h_\sigma e Z_\sigma \rho_{\mathrm{b}} j/9w^2 kT)t$, which can be easily deduced by inverse scaling procedure, Above expression clearly shows that there is a finite incubation time for the cathode failure by cathode edge contact area shrinkage due to voiding under the constant current operation, which is given by $\bar{t}_{INC} = 1/4\chi$, in normalized time and space domain. Similarly, we found an analytical expression for the cathode displacement (drift) under the FM-BC utilizing the constant current source program, which results not surprisingly exactly the same analytical expression that we obtained from the constant voltage source program, namely:

$$\bar{d}^{\mathrm{CC}}_{\mathrm{Drift}}(\chi,\bar{t}) = 0.661\chi\bar{t} + 0.126\bar{t} \tag{14}$$

where we have also used the end of the cathode shrinkage by voiding as a reference point for the normalized time scale for the development of cathode edge drift-displacement process. Hence, one can easily see from earlier equation that even under the zero applied electric field, as we have observed independently by simulating $\chi = 0$ experiment, the cathode edge-drift or displacement is possible under the free-boundary condition due to the capillary forces alone without having any external interference agent as employed in the constant voltage

experiments. The main reason behind this apparently peculiar behavior, which is rejected by some referees categorically because it is unobservable in standard test conditions, is solely connected to the natural trend of the system (Nichols and Mullins, 1965) to reach an equilibrium geometric configuration (faceting in the case of anisotropy) having minimum total surface Gibbs free energy (assuming that the bulk free energy and volume are invariant) driven by the global positive minimum internal entropy production (capillary force). The adverse effects of capillary forces on copper/dielectric interfacial void evolution had been studied by Choy and Kavanagh (2004) in axisymmetrical wire thinning by computer simulations. They have found that with zero electric field or with small field applied, a large void experiences a capillary instability which leads to open circuit failure. This is also contrary to general belief that the capillary forces may counteract the electron wind forces, such as that void growth by electron wind force is later healed or flattened out by capillary induced surface diffusion. Capillary forces may always act as a healing force, unless the surface stiffness function enters into the anomalous regime in strongly anisotropic systems, where it takes negative values along the certain directions (Ogurtani, 2006) and causes extreme instability.

Direct observation of capillary effect, which is simulated by FM-BC but not by R-BC, depends on the test condition at the cathode edge (i.e., electrical contact by mechanical means without soldering) otherwise on the physicochemical characteristics (poor adhesion/wetting) of the interface between cathode edge and the electrode material. However, both simulation experiments in the cathode drift stage, SOCV and CC, give the same results, because in the cathode drift stage they are all driven under the same constant current conditions. In the first situation it is artificially created by the switching operation, and in the second case it is developed naturally after the cathode shrinkage period.

One may immediately obtain the cathode drift velocity under the constant current operation by differentiating equation (14) and then applying renormalization and rescaling procedures, which result exactly the same relationship deduced previously. That relationship can be used to define the cathode failure time (CFT) by the cathode edge displacement if the specimen electrode contact configuration is similar to the Cu-damascene lines. Where the bottom surface of the cathode edge of the interconnect line is used to establish electrical contact pad through underlying vias. Then one writes the following expression for the cathode failure time denoted by $t_{\mathrm{CFT}}^{\mathrm{Drift}}(f)$ for a specified fractional resistance variation denoted by $f = \Delta R/R_0$ adapted by the test regulations, and the well known inverse relationship between the specimen resistance and the active cathode electrode cross section ($f \to \infty$ corresponds to the full coverage of the cathode contact cross section by the voiding)

$$t_{\mathrm{CFT}}^{\mathrm{Drift}}(f) = \frac{f}{1+f} L_{\mathrm{Via}} / V_{\mathrm{drift}}^{\mathrm{CC}} = \frac{f}{1+f} L_{\mathrm{Via}} 2h_{\mathrm{c}} \left\{ 1.98 \frac{D_\sigma h_\sigma e Z_\sigma \rho_{\mathrm{b}} j}{kT} + 3.4 \frac{\Omega_\sigma D_\sigma h_\sigma g_\sigma}{(2h_{\mathrm{c}})^2 kT} \right\}^{-1} \tag{15}$$

In the derivation of above equation, 'w' that appears in the original formula, Eq. (11) as a line width is now replaced by $2h_{\mathrm{c}}$, where h_{c} is the distance between the W-via electrical contact surface and the top surface of the interconnect line. L_{Via} is the dimension of the via contact area parallel the cathode edge displacement, assuming that it has a constant width in the perpendicular direction (the rectangular cross section). Similarly, this relationship also shows that if the sidewalls are dominant diffusion paths rather than the top surface or interface of the interconnect line then $2h_{\mathrm{c}}$ should be replaced by the line width w. Hence, in the EM dominating regime where the last term gives a negligible contribution to the CFT then the life time becomes linearly proportional with the line width and the current exponent becomes equal to $n = -1$ as observed by Hu et al. (1997).

It becomes obvious that the differences between the results of the constant voltage and the constant current experiments are negligibly small as far as the cathode drift phenomenon is concerned. The main difference comes from the form of the analytical functions that describes the time dependence of the cathode shrinkage processes at the cathode regions, which are given by Eq. (19) of recent work of Ogurtani and Akyildiz (2005) and Eq. (13) of this article, respectively.

In Fig. 4, the normalized incubation time for the cathode drift displacement under the constant current operation versus electron wind intensity parameter, $\chi = (0.001 - 50)$, is plotted on a double logarithmic scale, where the wetting parameter and aspect ratio are chosen as $\lambda = 0.8$ and $\beta = 20/3$, respectively. A linear regres-

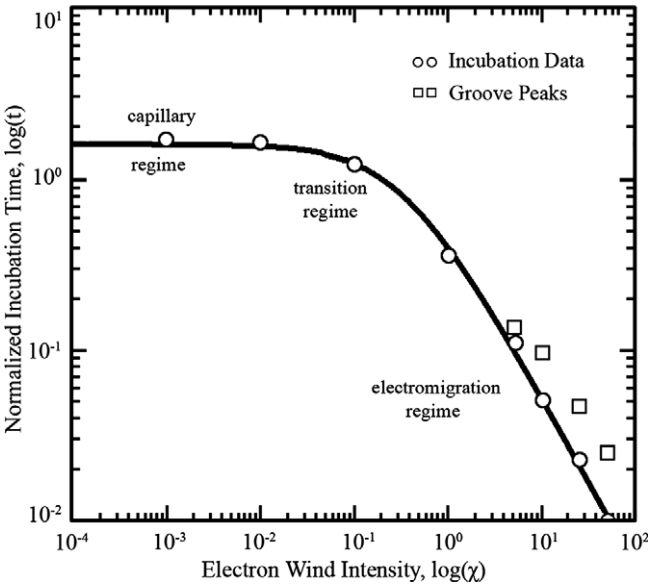

Fig. 4. Cathode drift displacement incubation time (or CCFT) versus electron wind intensity parameter plot on the double logarithmic scale, which clearly shows the existence of the capillary plateau and the EM regime under the constant current operation. There seems also a strong correlation between groove peaking associated with the current crowding and the incubation time in the EM regime. The solid curve is a modified hyperbolic function obtained by the inverse linear regression analysis.

sion analysis, which is applied to the inverse time versus electron wind intensity parameter, has resulted the following analytical expression after inversion procedure:

$$\bar{t}^{\mathrm{CC}}_{\mathrm{Incub.}}(\chi) \cong \bar{t}_{\mathrm{CCFT}}(\chi) = \frac{0.5774}{0.3219 + \chi} \quad \text{Incubation time for cathode edge drift} \tag{16}$$

Above expression is also plotted in Fig. 4, which shows an excellent match with the data points obtained from our computer simulation experiments under constant current condition. This modified hyperbolic function in log–log plot shows three distinct domains; the first region corresponds to the capillary dominating $\chi \leqslant 0.01$ plateau region, where the current exponent is equal to zero, $n = 0$ and the second linear region $\chi > 1$ where the applied electric field dominates the capillary effect, which shows a current exponent is equal to unity, $n = -1$ (the Black law). Between these two regimes the transition stage with varying current exponent lies. In Fig. 4, the plateau region has an upper bond described by $\chi \leqslant 0.01$ (top surface is active path: $\approx 10^8$ Am^{-2} where $h_c \approx 0.3$ μm), which corresponds to capillary regime, and $\chi \geqslant 1$ (top surface is active path: $\approx 10^{10}$ Am^{-2} where $h_c \approx 0.3$ μm) is the lower bond of the strictly electromigration dominating regimes, respectively. $\chi \cong 0.2$ roughly corresponds to knee point of the curve that describes the mid region of the transition stage.

The technical significance of the cathode drift incubation time becomes more clear if one designs an experimental test structure such that the face of the cathode-edge is used as an electrode contact area, and the elapsed time for the complete electric break down (the sharp resistance increase) as a measure for the evaluation of the interconnect failure time. Otherwise it has no practical significance in the determination of the life time of devices commonly used in microelectronic industry, such as Cu-damascene design with Cu-via or W-via as electrical contact means.

Now we may transform above equation into the real time and space domain by inverse scaling which results following relationship for the complete cathode failure time (CCFT) due to the cutoff in the applied voltage by the cathode contact area shrinkage by voiding

$$t^{\mathrm{CC}}_{\mathrm{CCFT}}(\chi, w) = 0.576 w^2 \left[3^2 \frac{D_\sigma h_\sigma e Z \rho j}{kT} + 0.322 \times 3^4 \frac{\Omega_\sigma D_\sigma h_\sigma g_\sigma}{w^2 kT} \right]^{-1} \tag{17}$$

The CCFT time as we mentioned previously corresponds to the onset of the cathode drift phenomenon by voiding, and it was called as the incubation time for the cathode edge displacement. This general expression, which covers the whole domain of capillary and EM dominating regions including the transition stage, can give following two formulas, which represent the both domains very accurately. However, the practical significance of the cathode failure time associated with the cathode shrinkage by voiding at the cathode edge-face of the interconnect line may be very limited if one uses the Damascene configuration where the electrical contact are established by vias at the bottom face of the cathode edge, and having top surface acting as a dominant diffusion path because of no capping. Then, Eq. (15) developed above should be seriously considered in the prediction of CFT for the copper damascene lines having W-via or Cu-via as electrical contact pads and voiding takes place in the metal line including the upper part of the via (trench-voiding). While doing that one should only pay a special attention to the possible drift-diffusion paths by relying on the experimental observations on test structures using TEM or HVSEM techniques to determine the exact locations of the cathode void formations, which is vital for the realistic estimation of h_c that is a very critical parameter in the prediction of CFT. Hence, one may write

$$t^{CC}_{CCFT}(\chi, w) = 6.4 \times 10^{-2} w^2 \left[\frac{D_\sigma h_\sigma e Z_\sigma \rho_b j}{kT}\right]^{-1} \quad \text{EM dominating region; } \chi \geqslant 1 \text{ Cathode Shrinkage} \tag{18}$$

and

$$t^{CC}_{CCFT}(\chi, w) = 2.2 \times 10^{-2} w^4 \left[\frac{\Omega_\sigma D_\sigma h_\sigma g_\sigma}{kT}\right]^{-1} \quad \text{Capillary dominating region; } \chi \leqslant 0.01 \text{ Cathode Shrinkage} \tag{19}$$

where the critical current densities associated, respectively, with the lower and upper bonds of the EM and capillary regimes for the CCFT can be easily calculated from the critical values of the normalized electron wind intensity parameter obtained from Fig. 4 as: $\chi_{EM} = 1$ and $\chi_{CAP} = 0.01$, which results

$$J^{CCFT}_{EM} \cong 9 \frac{\Omega_\sigma g_\sigma}{w^2 e Z_\sigma \rho_b} \text{ and } J^{CCFT}_{Cap.} \cong 0.09 \frac{\Omega_\sigma g_\sigma}{w^2 e Z_\sigma \rho_b} \tag{20}$$

The first marginal current density parameter J^{CCFT}_{EM}, which marks the onset of the EM dominating regime for the drift displacement kinetics, where there is a linear connection between the drift velocity and the applied current density, is almost two orders of magnitude greater than the upper bond of the capillary dominating regime. A close inspection of Eq. (20) clearly shows that the surface specific Gibbs free energy density associated with the interfacial layer plays an exceptional role for the determination of the onsets of the EM and capillary dominating regimes, where a substantial reduction in the CCFT takes place compared to the those values obtained by extrapolating the accelerated test data down to the actual device operating conditions; namely, much lower applied current densities and operating temperatures. These threshold levels may be depend on the operating temperature due to the possible temperature dependence of intrinsic properties of the interconnect material such as specific bulk electrical resistivity, ρ_b, as well as the metal/liner and metal/dielectric interfaces $(Z_\sigma, g_\sigma, D_\sigma, h_\sigma)$. The most important and effective metallurgical control parameter is the specific surface Gibbs free energy, which should be as small as possible. The data related to the GB groove peaking times (GPT) for various electron wind intensities is also plotted in Fig. 4, which shows that there is a very close correlation between GPT, where the strange groove tip velocity inversion (healing effect) takes place (Ogurtani and Akyildiz, 2005) and the cathode drift onset time, which may be called as the cathode drift incubation time.

The original definition of the catastrophic cathode failure time (CCRT) due to cathode contact area shrinkage by voiding adapted in this paper might be misleading for those attempting to use Eq. (17) on the copper damascene configuration, in which electrical contact is furnished by vias. This opposes our presumption that the electrical contact to the specimen is established at the cathode edge by the DMCE without soldering. However, this concept of CCFT by voiding still may be applied to Cu-Damascene interconnect line under very special conditions, namely; the via regions are the natural extension of the test specimen similar to Cu-via and the surface is capped with metal coating (CoWP, CoSnP, or Pd) to inhibit SN_x coated top interface from acting as

a fast drift-diffusion path (Hu et al., 2002, 2004; Fischer et al., 2002). According to experimental findings, (Hu et al., 2002), mostly the via-bottom void is observed in the capped samples, which is a strong indication that the sidewall and via-bottom interfaces may play dominate diffusion paths rather than the top surface or interfacial layer. Furthermore, this also shows that not the cathode edge displacement but the via contact area shrinkage by voiding (via-voiding) is the primary cause for the electrical break down. Then, CCRT concept mentioned above may be employed for the prediction of the cathode failure time by careful evaluation of the effective path length $\hat{w}$, which may be replaced by the dimension of the via parallel to the longitudinal direction of the line, especially in those cases where the interfacial layer between Cu-via and the under liner W-Mo or Cu interconnect line C and W-via shows rather poor adhesion (wetting) properties (Fischer et al., 2002).

4. Discussions

Above mentioned test configuration of the interconnect line resembles the famous experimental set-up by Blech and Kinsborn (1975), in the measurement of the drift velocity at the cathode edge with one exception. Namely, in the present computer simulations the electrical current injection is established not only by the shunt effect of the substrate but also through the DMCE at the anode and cathode-edge faces, with and without soldering, respectively. This configuration allows us to use insulating and free boundary conditions at the anode and cathode edges, respectively. The present study puts the main emphasis on the evolution behavior of bi-crystals and bamboo-like interconnect lines when the upper surface and/or the sidewalls become dominant mass transport paths for the drift-diffusion under the action of EM and capillary forces. In certain experimental configurations the cathode void growth occurs in step-wise fashion by the special type of grain thinning process that proceeds from top surface down to bottom after the initial short period of time where an edge displacement mechanism is operating, as in the case of Liniger et al. (2002) experiments. The cathode voiding by grain thinning phenomenon, which dominates overall behavior of the above cited studies, may not be evaluated with a great confidence by the analytical expressions such as Eqs. (15) or (17) obtained by the present computer simulation unless one has true understanding of this mechanism. The effect of the line width on void growth rate was also investigated by Liniger et al. (2002) and found to be negligible, and they immediately claimed that it was consistent with a top surface-diffusion dominated model for void growth. However, they did not make any attempt to check whether there is any thickness dependence to verify that the top and/or bottom surfaces were the primary diffusion paths. As far as the validity of FM-BC simulations is concerned the specific type of the surface paths is unimportant and can be upper and lower surfaces or interfaces, even the lateral sides and edges of the interconnect line.

According to experimental study of Hu et al. (1997) on pure copper interconnects in the temperature range of 221–394 °C by using both drift-velocity and resistance measurements in narrow (0.25 μm) bamboo-like grain structures, there is a linear relationship between failure lifetime and metal line width, as predicted by Eq. (15) because the sidewalls are active diffusion paths, in addition to the low value obtained for the activation enthalpy of EM 0.81 ± 0.05 eV. Based on these results, they have suggested that the mass transport of Cu primarily occurs along the sidewall surfaces of the line during EM measurements, and the measured activation enthalpy is for the drift-diffusion on Cu lateral surfaces, which were exposed to air and other contaminations, since they have used temperatures ranging from 221 °C to 394 °C in a vacuum furnace with a chamber pressure of 20 Torr. Here, one should recall that the reported EM activation energy of Cu film with a clean surface, deposited and tested in ultra-high vacuum condition is about 0.47 eV while vacuum deposited films that were air exposed gave a value of 0.79 eV. (Park and Vook, 1991, 1993). The physical configuration of these Cu lines resembles our simulation set-up, and they were sandwiched between the top and bottom Ta layers. The Cu test lines were designed to be 0.25, 0.5 and 1.0 μm wide and overlapped the W bars of 1.0 μm. The experimental specimen configuration employed in above cited studies can be easily examined by using Eq. (15) as far as the cathode failure time concept, which is a linear function of the line width as observed by Hu et al. (1997) is concerned. According to the definition of these authors, the mean failure time $\langle \tau \rangle$ is approximately the time for the mass depletion (voiding) at cathode end of the line, which is taken as 0.7 μm void formation for the 0.25 μm wide line, without considering the part of the void already formed in their reservoir in their data analysis. Hence, in the application of the formula equation (15) by taking $f \to \infty$, where the initial nucleation and

growth time of the void in the reservoir is automatically enters into our definition of cathode failure time, therefore in the effective cathode contact length should consider the reservoir overlapping, which means $\Delta L_f \cong 0.7 + 1.0 = 1.7$ μm. In Fig. 5, the mean cathode failure time (MCFT) data, reported by Hu et al. (1997) in their Fig. 7. for 0.25 thick specimen, is plotted on a semi-logarithmic scale, the EM activation enthalpy is calculated by the linear regression analysis and the results are presented in Table 1. In this figure, the solid line, which is designated as capillary, is associated with the capillary contribution to the MCFT, which is two orders of magnitude smaller than the electromigration effect as mentioned previously. The activation enthalpy of the surface drift-diffusion obtained from the fitting of equation (15) to the experimental points resulted an excellent agreement with the EM-activation energy obtained by the linear regression analysis after the kT correction.

In later studies Hu et al. (1999) employed a completely different test specimen configuration, where the top surface and sidewalls were free surfaces and exposed to environment whereas the bottom surface was covered by Ta diffusion barrier, and found that the drift velocity decreases with the line width, goes through a minimum at $w_0 = 1$ μm, and then increases to a constant value in narrow (0.15 μm) bamboo-like and near-bamboo structures (0.5 μm). Drift velocity according to Eq. (11) is a hyperbolic function of the line width in EM dominating regime, which is also proved by the analysis of Hu et al. (1999) data as presented in Fig. 6. All these experimental results suggest that the mass transport of Cu during EM primarily occurs along the free surfaces, whether they are sidewalls and/or the top surfaces of the interconnect lines, when the rest is coated by metal liner with very low EM induced mass transport properties.

In Fig. 6, the theoretical curves associated with the cathode drift-displacement velocity versus line width are plotted by employing Eq. (11), for two different test temperatures 528 and 587 K. In the evaluation of the theoretical curves the following data resulted the best fit for the experimental points: $D_0^{\mathrm{Cu}} \cong 1.0 \times 10^{-5}\ \mathrm{m^2\ s^{-1}}$, and $H_{\mathrm{Cu}} = 1.00$ eV at applied current density given by $J = 1.5\ \mathrm{MA\ cm^{-2}}$. The predominant diffusion paths are sidewalls and the top surface, which are all exposed to environmental conditions. The bottom surface

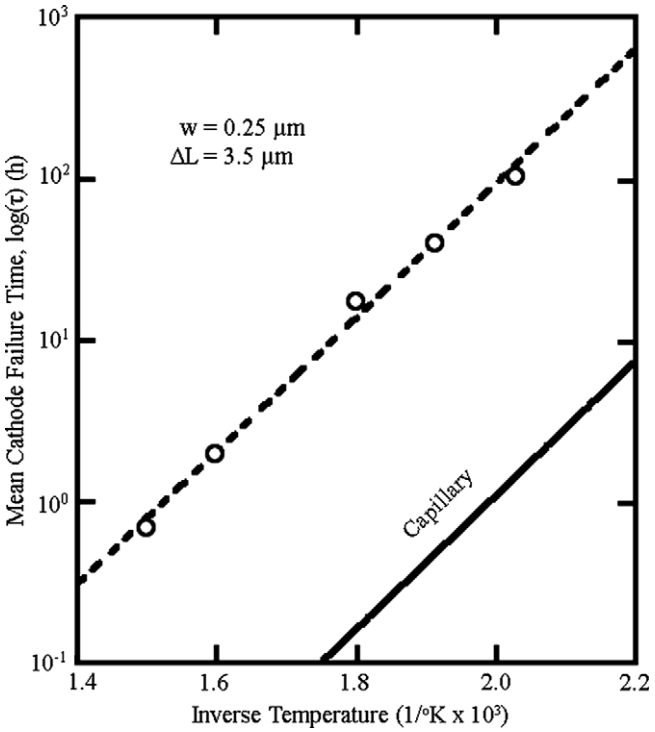

Fig. 5. The cathode failure data reported by Hu et al. (1997) is plotted as a function of inverse absolute temperature on a semi-logarithmic scale for 0.25 μm thick specimen. The theoretical best fit curve according to Eq. (15) is also presented in the graph by a dash line, which yields. Data: $Z^*_{\mathrm{Cu}} = 12$, $H_{\mathrm{Cu}} = 0.87$ eV, $D_0^{\mathrm{Cu}} = 0.5 \times 10^{-5}\ \mathrm{m^2\ s^{-1}}$, and $J = 2.5\ \mathrm{MA\ cm^{-2}}$.

Table 1
Experimental data analysis in terms of cathode drift velocity versus temperature and current density for Copper interconnects, where $Z_{Cu} = 12$.

Reference		Liniger et al. (2002)	Hu et al. (1999)	Hu et al. (1997)	Khenner et al. (2001)
Specimen characteristics					
Voiding mode		Grain thinning	Edge displacement	Edge displacement	Edge displacement
Structure		Bamboo like	Bamboo like	Bamboo like	Poly-crystalline
Preparation[a]		EP	EGE	EGE	*
HT[b]	Type _	NA	A	A	*
	T (°C)	*	400	400	*
	t (h)	*	3	3	*
Length (μm)		100	200	200	0.50
Width (μm)		0.18	0.15	0.25	0.50
Thickness (μm)		0.3	0.3	0.17	2D
T (°C)		230–350	255–405	221–394	600
J (MA cm^{-2})		1.8	1.5	2.5	200
Bottom		Ta	Ta	Ta	2D
Sidewalls		Ta	Free	Free	GB
Top[c]		Free	Free	Ta	2D
Literature					
Activation enthalpy (eV)		0.9 ± 0.1	0.9	0.81 ± 0.05	*
Surface diffusivity (m^2 s^{-1})		2.6×10^{-5}	*	*	*
Current exponent		−1	−1	−1	−1
Computer work					
Effective path (μm)		2×0.30	0.12	0.75 (void) 1.00 (reservoir)	0.5
Activation enthalpy (eV)		1.00	1.00	0.87	0.87
Drift velocity (μm/hrs)		*	*	*	3.47×10^6
Surface diffusivity (m^2 s^{-1})		1.0×10^{-4}	1.0×10^{-5}	0.5×10^{-5}	*
Regression analysis					
Standard error, σ		0.089	0.337	*	*
Apparent activation enthalpy (eV)		0.955 (+0.048)	0.954 (+0.052)	0.822	0.94
Drift velocity (μm/h)		2.43×10^7	3.39×10^7	*	4.6×10^6
Cathode failure time constant (h) t^{∞}_{CFT}		*	*	4.64×10^{-7}	*

[a] EP: electroplated, EGE: e-gun evaporator.
[b] HT: Heat Treatment, A: Annealed, NA: Not annealed.
[c] UC: uncoated, CP: capped with CoWP, Cu/Ta: Interface.
[d] E: Experiment, T: Theory.

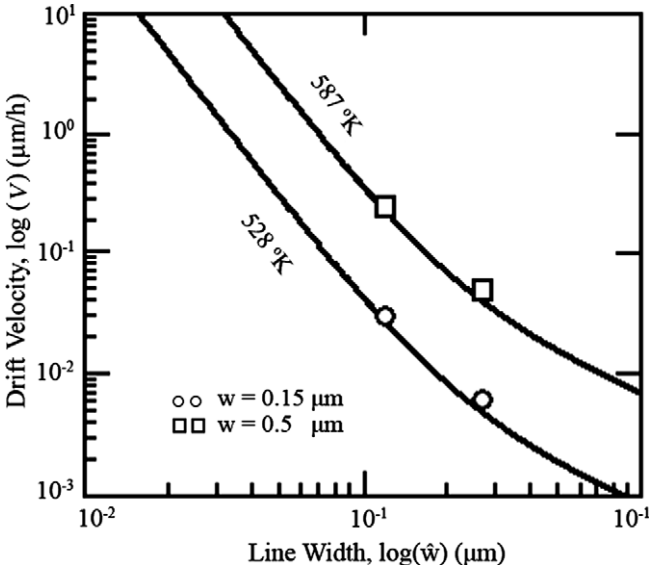

Fig. 6. The cathode drift-displacement velocity versus line width is plotted for two different temperatures 528 and 587 K and line widths using Eq. (11). On the same graph experimental observations of Hu et al. (1999) are also presented for comparison, which show almost perfect agreement with the theoretical curves. Data: $Z^{s}_{Cu} = 12$, $D^{Cu}_{0} \cong 1.0 \times 10^{-5}$ m^2 s^{-1}, $H_{Cu} = 1.00$ eV and $J = 1.5$ MA cm^{-2}.

has Ta under liner as a diffusion barrier. On the same graph experimental observations of Hu et al. (1999) are also presented for comparison, which show almost perfect agreement with the theoretical curves. During the calculation of the theoretical curves the three parallel acting diffusion paths (concurrent) are considered in the data acquisition, which may easily formulated by following an ad hoc procedure, which is mostly used in reaction kinetics for the concurrent as well as the consecutive reactions (Yeremin, 1979) to obtain the effective reaction rate constant by electrical network analogy. Hence, the effective diffusion path parameter is given by $1/\hat{w} = 1/w + 1/2h_s$, that results: $w = 0.15\ \mu m \rightarrow \hat{w} = 0.12\ \mu m$ and $w = 0.5\ \mu m \rightarrow \hat{w} = 0.27\ \mu m$, where the specimen height is $h_s = 0.3\ \mu m$. This method of path length evaluation is exactly analogue to the expression Eq. (4b) obtained *ad hoc* fashion and used extensively by Hu et al. (1999, 2002a,b) in their papers. We have also used the reflection symmetry property of our mathematical model in the evaluation of the upper surface effective diffusion path length, which is equal to $2h_s$. The argument behind this approach may be easily anticipated by simply forming a new specimen by reflecting the sample with respect to the Ta liner, and then simulate the problem by letting upper and newly formed lower surfaces as diffusion paths. The result is simply replacing the original height by the height of the new sample, namely $2h_s$, since now Ta under layer plays the role of R-BC. The same factor of 2 also appears in above cited references but in a completely different context or argument, which may be easily seen by close inspection of their drift velocity formulas.

The following input parameters for copper interconnect metallic lines are used in connection with the numerical evaluations of our analytical expressions for the cathode drift velocity denoted by Eq. (11) and CCFT given by Eq. (16): $\Omega_\sigma = 1.66 \times 10^{-29}$ m^3, $h_\sigma = 2.56 \times 10^{-10}$ m, $\rho_{Cu} = 3.89 \times 10^{-8} \Omega$ m at 330 °C, $g_\sigma = 1.725$ J/m^2 (Smithells, 1967). According to our previous work (Ogurtani and Oren, 2004) on the copper interconnects, the mean time to failure (MTF) evaluations using the analytical expression, $Z_\sigma = 12$ gives much better results in the present of experimental observations for the copper surface layers, which are exposed to unavoidable contaminations during the manufacturing and the EM testing procedures.

Since the kinetics of cathode drift-displacement is a strong function of temperature (almost exponential), one can obtain very accurate information concerning the activation enthalpy of drift-diffusion from the void drift velocity versus inverse absolute temperature data. In Fig. 7, the experimental data taken from Fig. 2 of Hu et al. (1999) on the cathode drift velocity for copper interconnect lines having, respectively, $w = 0.15\ \mu m$ ($\hat{w} = 0.12\ \mu m$) and $w = 0.50\ \mu m$ width ($\hat{w} = 0.27\ \mu m$), and $h = 0.3\ \mu m$ thickness, and exposed to different test temperatures are plotted on a semi-logarithmic scale. The results of our linear regression analysis

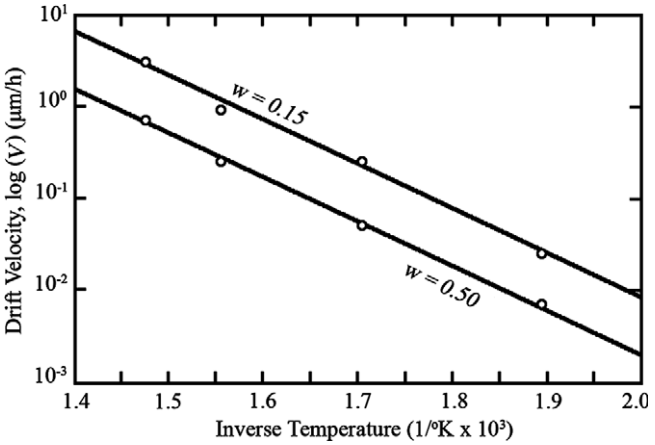

Fig. 7. The cathode drift velocity versus inverse absolute temperature obtained from Hu et al. (1999) is plotted on a semi-logarithmic scale for two different line widths. Theoretical curves calculated from Eq. (11) are also presented for comparison, these show excellent match with the line deduced from the linear regression analysis. Data: $Z^s_{Cu} = 12$, $D^{Cu}_0 \cong 1.0 \times 10^{-5}$ m^2 s^{-1}, $H_{Cu} = 1.00$ eV and $J = 1.5$ MA cm^{-2}.

applied on their raw data, in terms of apparent activation enthalpies and intercepts are presented in Table 1. In the same plot, the theoretical cathode drift velocity relationship denoted by Eq. (11) is also presented using the experimental information such as the specimen effective path length $\hat{w}$, and the applied current density by adjusting the surface diffusion activation enthalpy H^s_{Cu} and the temperature independent cofactor denoted by $[\hat{w}^{-1}(D_0 h_\sigma Z_\sigma)\rho_b ej]$ to get the best fits. A close inspection of Eq. (11) in connection with the almost perfect straight-line behavior of the experimental data with high confidence limits immediately reveals the fact that, those authors were testing their specimens under the EM dominating regime. The fitting of our analytical expression to those experimental data points results a consistent activation enthalpy of the surface diffusion such as $H^s_{Cu} = 1.00$ eV. In addition, the surface diffusion constant, $D^{0,s}_{Cu} = 1.0 \times 10^{-5}$ m^2 s^{-1}, obtained previously using the calculated value of CEPL for the 0.15 μm and $w = 0.50$ μm wide copper lines in the temperature independent cofactor in Eq. (11), resulted excellent match with the data presented by Hu et al. (1999) as can be seen in Fig. 7.

Strangely enough the linear regression analysis of the data produced by Hu et al. (1997) and Liniger et al. (2002) give the same and consistent results, namely $H^{App}_{Cu} = 0.953$ eV and 0.955 eV with the standard errors $\sigma = 0.2$ and 0.089, respectively. Even though those two experiments they do have completely different specimen configurations, and the line width dependencies. Hu et al. (1997) stresses on the free sidewall surfaces dominating Cu electromigration transport having linear dependence on the line width, and Liniger et al. (2002) definitely has the grain thinning mechanism operational in their specimens, and the top free surface was claimed to be the main diffusion path since no dependence found on the specimen width. Unfortunately, it seems that both authors did not pay attention on the proper application of the statistical analysis on their data, which can be immediately anticipated by looking at Fig. 3 of Hu et al. (1999). They both reported tentative values such as 0.9 eV for the surface diffusion activation enthalpy. The main difference between these two activation enthalpy values and the theoretical activation enthalpy obtained by Eq. (11) comes from the fact that the slope deduced by the linear regression analysis represents the apparent activation enthalpy, which overlooks the contribution of $1/kT$ in the mobility expression known as Nernst–Einstein relationship in the literature. As we demonstrated elsewhere (Ogurtani and Oren, 2004), the apparent activation enthalpy may be defined by the following expression: $\tilde{H}^s_{Cu} \equiv -\partial \ln(V_{drift})/\partial(1/T) = H^s_{Cu} - kT$, where, we have neglected the temperature dependence of others parameters, which enter the theoretical expression, namely: the specific surface Gibbs free energy, the conductivity, and possibly the effective charge, etc. The contribution from kT amounts to 0.048–0.052 eV at the temperatures of about 560–600 K, which correspond to the mean values of the temperature ranges employed by those authors in their experiments. Hence, the true activation enthalpy of the surface diffusion of copper in both experimental test conditions, which may heavily dependent on the level of contamination during the sample preparations as well as the EM testing conditions, amounts to about

1.0 eV as we obtained from directly from the fitting of our theoretical expression on their data. As far as the D^0_{Cu} value is concerned, both research groups have employed completely different test sample configurations in their experiments. Test samples used by Hu et al. (1999) supported by Ta under liner, otherwise upper and lateral surfaces are completely exposed to air, and they also demonstrated that there is line width dependence.

Liniger et al. (2002), relying on SEM micrographs of the bamboo-like 0.18 μm wide lines tested in series at 260 °C with $J = 1.8\ \mathrm{MA}/\mu\mathrm{m}^2$, has stated that the void growth up to 9 h appears to occur by edge displacement. However, the grain ahead of the void front shows thinning from the grain surface from tests times 9–46 h. Once the grain empties out, the next grain again thins from the grain surface from 46 to 74 h. As we mentioned previously it may not be proper to apply our formula denoted as Eq. (11) directly to the cathode drift velocity data, which is obtained by smoothening the displacement versus time plot deduced for 0.18 μm wide line that shows stepwise jerky advancement due to the sporadic behavior of the grain tinning mechanism. Nevertheless, it might be beneficial to apply Eq. (11) to their experimental results to see the discrepancies between the cathode edge displacement by edge voiding and the sporadic displacement by the grain thinning associated with the top surface drift-diffusion.

The analysis of the data presented by Liniger et al. (2002) has certain pin holes, which are closely related to the grain thinning mechanisms operating in their experiments. The straight usage of the effective line thickness $\hat{w} = 0.60$ μm in Eq. (11), which is deduced for the cathode edge displacement mechanism by assuming that only the top free-surface contributes to the mass transport that generates void at the cathode end, furnished about one order of magnitude shift towards the low values of the edge drift velocities, using above obtained diffusion constant $D^{0,s}_{Cu} = 1.0 \times 10^{-5}\ \mathrm{m}^2\ \mathrm{s}^{-1}$ and the activation enthalpy rather than $D^{0,s}_{Cu} = 1.0 \times 10^{-4}\ \mathrm{m}^2\ \mathrm{s}^{-1}$, which gives the best fit. This awkward situation however does not alter the apparent activation enthalpy of diffusion obtained for the free but contaminated copper surface dominant experiments cited above. On the other hand the line width independency of Liniger et al. (2002) experimental results does not contradict to our speculation since only the specimen thickness enters into the theory when the top and/or bottom surfaces are active diffusion paths.

In Fig. 9, the cathode drift-displacement velocity versus current density is plotted for various temperatures for copper interconnect thin films having $w = 0.15$ μm by utilizing Eq. (11), where the same diffusion parameters obtained from analysis of Figs. 6 and 7 were employed: $H^s_{Cu} = 1.00$ eV, $D^{0,s}_{Cu} = 1.0 \times 10^{-5}\ \mathrm{m}^2/\mathrm{s}$ and $Z^s_{Cu} = 12$. On the same plot experimental results of Hu et al. (1999) for the same line width is also presented for comparison and the excellent agreement between the theory and their experimental findings can be clearly seen. The computer simulation findings of Khenner et al. (2001) as well as its application on Hu et al. (1999) data are presented after making proper rescaling procedure. Theoretical line drawn at 600 K using the diffu-

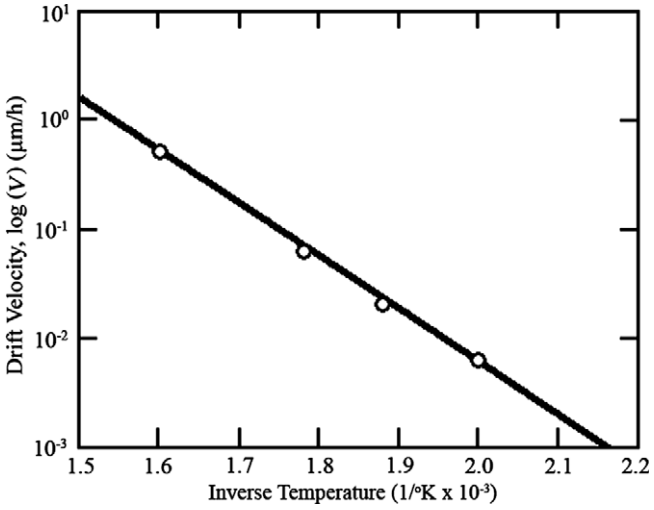

Fig. 8. The cathode drift velocity versus inverse absolute temperature obtained from Liniger et al. (2002) is plotted on a semi-logarithmic scale. The theoretical curve is calculated from Eq. (11). Data: $Z^s_{Cu} = 12$; $H^s_{Cu} = 1.0$ eV, $D^{0,s}_{Cu} = 1.0 \times 10^{-4}\ \mathrm{m}^2/\mathrm{s}$.

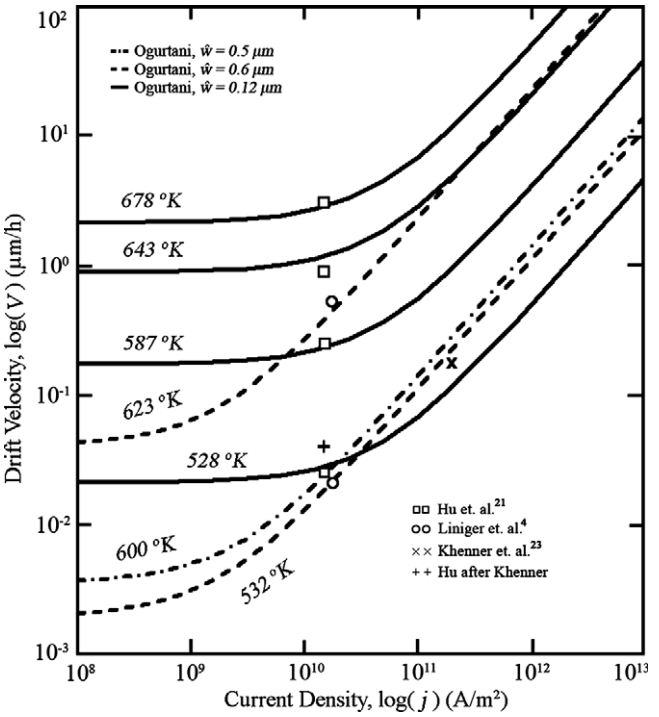

Fig. 9. The cathode drift-displacement velocity versus applied current density is plotted on a double-logarithmic scale using Eq. (11), for various temperatures for a copper bamboo-like interconnect having exactly same microstructure used in both experiments. Data: $Z^{s}_{Cu} = 12$, $H^{s}_{Cu} = 1.00$ eV, $D^{0,s}_{Cu} = 1.0 \times 10^{-5}$ m^2/s (Hu et al., 1999), $D^{0,s}_{Cu} = 1.0 \times 10^{-4}$ m^2 s^{-1} (Liniger et al., 2002).

sion coefficient obtained in this work resulted excellent match with the data obtained by Khenner et al. (2001) and Hu et al. (1999) on the near bamboo line having a line width of 0.5 μm.

Nathan et al. (2000) and Khenner et al. (2001) have employed a constant voltage set up ($U^{+} = -U^{-} = 5 \times 10^{-3}$ V) for their square computational box 0.5 μm × 0.5 μm, which corresponds a electric field intensity given by ($E = 2 \times 10^{4}$ Vm^{-1}), in their computer simulations, carried out at 600 K by using a level set method. Nathan et al. (2000) have claimed that during the cathode edge displacement, the current density variations in the interconnect may be approximated by 2.7×10^{10}–1.7×10^{10} A/m^2. Similarly they have also stated that by tuning the applied voltage differential to their box, they have succeeded to maintain a constant current density around $j = 1.5 \times 10^{10}$ A/m^2 during their simulations. Unfortunately, both authors working in the same research group have reported these figures for the current densities as outlined above in their joint papers However, this can hardly to be conceivable in the presence of applied electric field intensity used in their computation box, even using their arbitrary selected values for the conductivities of copper and the under layer (like Ta, TiN or TaN). Khenner et al. (2001) used $\sigma_{Cu} = 10^{8}(\Omega\,\mathrm{m})^{-1}$ and $\sigma_{Ta} = 10^{7}(\Omega\,\mathrm{m})^{-1}$, and Nathan et al. (2000) employed $\sigma_{Cu} = 7.5 \times 10^{6}(\Omega\,\mathrm{m})^{-1}$ and $\sigma_{Ta} = 7.5 \times 10^{6}(\Omega\,\mathrm{m})^{-1}$. According to a simple calculation, one may show that the starting values for current densities in constant voltage experiments simulated by them should be given by $J_{Start} = \sigma_{Cu} \times E = 2.0 \times 10^{12}$ A m^{-2} and $J_{Start} = \sigma_{Cu} \times E = 1.5 \times 10^{11}$ A m^{-2}, respectively. Under any circumstances there is at least one or two orders of magnitude discrepancies in current densities which cannot be accounted for in these articles. The actual starting current density for copper interconnects for this applied electric field intensity is given by $J_{Start} = 5.14 \times 10^{11}$ A m^{-2} at 600 K using the tabulated values of the specific resistivity at 293 K and the thermal resistivity coefficient of copper, as it is done in our numerical work. Khenner et al. (2001) obtained $V_0 = 3.47 \times 10^{6}$ μm h^{-1}, and $H^{s}_{em} = 0.87$ eV, where the effective charge is assumed to be $Z^{s,Kh}_{Cu} = 5$. The calculated value of the drift-displacement velocity from these figures amounts to $V_{drift} = 0.175$ μm h^{-1} at 600 K, compared to the experimental value of 0.04 μm h^{-1} at 587 K which may be computed from $V_0 = 4.6 \times 10^{6}$ μm h^{-1} and $H^{s}_{em} = 0.94$ eV. These figures were referred by Khenner et al. (2001) in citing the work of Hu et al. (1999), in order to justify their

agreements. This experimental point is also marked in Fig. 9, which shows good agreement with our findings. In order to compare EM activation energy and the associated drift-velocity constant V_0 obtained by Khenner et al. (2001) under the constant voltage application, with the results of our present computer simulations, the actual current density ($E = 2 \times 10^4$ V m^{-1}) should be rescaled by the ratio of $\{Z^{s,\mathrm{Kh}}_{\mathrm{Cu}}/Z^{s}_{\mathrm{Cu}} = 5/12\}$, which gives $J_{\mathrm{Scaled}} = 2.14 \times 10^{11}$ A m^{-2}. The drift velocity $V_{\mathrm{drift}} = 0.175$ μm h^{-1} calculated above at 600 K is plotted in Fig. 9 with respect to the rescaled current density. Here, we have also draw a curve using Eq. (11) in connection with our system parameters and the surface diffusion coefficient obtained at 600 K for a copper interconnect of 0.5 μm wide, having bamboo like microstructure. The excellent agreement obtained between the prediction of our formula for the constant current application and the reported values of Khenner et al. (2001), seems to be too good to believe that it may be fortuitous after considering our pain taking rescaling procedure.

5. Conclusions

In the present computer simulation studies three important analytical relationships are obtained by inverse scaling procedures, which may have useful technological applications in microelectronic industry. Two of them deal with the cathode failure time (CFT) associated with the surface drift diffusion driven by capillarity and electromigration forces that are causing cathode voiding and thinning in thin film metallic interconnect line having bamboo structures. As far as the cathode electric contact breakdown phenomenon by the surface diffusion assisted voiding is concerned, two distinct mechanisms are elaborated and formulated in this paper. The cathode failure times associated with these mechanisms are presented analytically by Eqs. (15) and (17), which may be employed for two different and distinct cathode electrode configurations mostly used in the microelectronic industry and in the reliability test laboratories (Tu, 2003), respectively, for the Cu-damascene (Cu-via or W-via) and the modified Blech type cathode contact structure as mentioned previously. Third relationship, which is given by Eq. (11) presents an analytical connection for the cathode displacement drift velocity (CDDV) by cathode voiding and thinning under the constant current operation. This connection also shows two distinct contributions, namely electromigration and capillarity predominating regimes. The capillary dominating regime has a very strong dependence on the size effect such as the line width or thickness w^3 rather than w as in the EM dominating regime. Importance of the capillary forces on the CDDV can be easily appreciated from Fig. 9., which clearly shows that most of the test structures and the operation conditions are in the range of the transition region, and rather close to the capillary plateau upper edge.

As far as the current density dependence of CFT is concerned, the relationship Eq. (17) can be directly applicable to the those test structures where the electrical contacts are established at the anode and cathode faces, and the cathode voiding and edge thinning takes place predominantly by the mass diffusion along the paths such as sidewalls and/or upper and lower surfaces including GB leakage. In that case, there are two different regimes, which result completely different current exponents above ($\chi \geqslant 1$) and below the electron wind intensity threshold levels ($\chi \leqslant 0.01$), and yields $n = -1$ and $n = 0$, respectively. The first regime is governed by the first term in Eq. (17), namely EM dominating stage, and the capillary regime is controlled by the second term. At the present microelectronic applications, as far as the size of the interconnect lines, the applied current densities and operating temperatures are concerned the contribution of the capillary term to CFT is completely negligible as can be seen from Fig. 5, and it is about two orders of magnitude smaller than the EM contribution. However, the capillary regime may be critical for the device operation and reliability if one goes down to the nanometric interconnects lines, in the future practices. Since the capillary dominating regime in the case of CFT has very strong dependence on the size effect such as the line width or thickness w^4 rather than w^2 as in the EM dominating regime. The change over current density between these two regimes even though spans rather a large range but still may be characterized roughly by the following expression: $j_{\mathrm{thr}} = 1.7156 \times \Omega_\sigma g_\sigma/(w^2 eZ\rho_{\mathrm{b}})$, which is called as the knee-current density, and it should be as small as possible for the benefit of CTF. Hence, one should try to select those materials as underlayers that one could be able to modify the properties of the interfacial layer, namely the specific surface Gibbs free energy, which should be as low as possible. This may be achieved by during the material design procedures such as the selective doping with impurities such as a trace amount of Zn in Cu that shows extensive segre-

gation or adsorption characteristics at the surfaces and in the interfacial layers, which causes reduction in the specific surface Gibbs free energy (Ogurtani, 1975).

The technological significance of the cathode failure time due to cathode voiding (via-voiding) at the cathode edge-face of the interconnect line defined by Eq. (17) may be very limited if one uses the Damascene configuration where the electric contacts are established at the lower surfaces of the anode and cathode edges of the interconnects lines having top surface acting as dominant diffusion path because of no capping (trench-voiding), as it was the case of Hu et al. (1997) and Fischer et al. (2002). Then, Eq. (15) developed above should be seriously considered in the prediction of CFT for the copper Damascene lines having W-via or Cu- via as electrical contact pads. While doing that one should only pay a special attention on the possible drift-diffusion paths by relying on the experimental observations on test structures using TEM (He et al., 2004) or HVSEM techniques to determine the exact locations of the cathode void formations, which is vital for the realistic estimation of h_c that is a very critical parameter in the quantitative prediction of CFT.

These diffusivity figures deduced from the present studies are very close to the results obtained by Ogurtani and Oren (2004, 2005) from the intergranular void dynamics simulations, ($\widehat{Z}_{Cu} = 12$ and $D_{Cu}^{Surface} = 5.85\times 10^{-5}\exp(-0.95\,eV/kT)\,m^2/s$) for the surface diffusion of internal voids having some minor contaminations pick up during the grain boundary void interaction period and/or at the nucleation stage. Where, they have analyzed almost all experimental data available in the literature related to aluminum and copper having bamboo and near-bamboo structures, utilizing the model developed by them for the MTF, associated with the internal voids drifting and interacting with the grain boundaries under the capillary and EM forces, in bamboo structures.

The cathode failure of interconnect line, which occurs by a very special grain thinning mechanism as observed by Liniger et al. (2002) that proceeds from the top surface down to bottom needs serious attention theoretically as well as in the computer simulations programming (Choy and Kavanagh, 2004). The theory advocated by Glickman and Nathan (1996) and his group cannot explain this top to toe grain thinning by their proposed vertical grain boundary grooving model coupled with cathode edge surface diffusion using neither type-A nor type-B mechanisms, which is simulated by Nathan et al. (2000) and Khenner et al. (2001) in polycrystalline samples, since grain boundary grooving no longer takes place along the those GB-planes parallel to longitudinal axis of the specimen rather proceeds top to bottom and where the active GB-planes are perpendicular to the direction of electromigration, similar to our configuration adapted in this work. Therefore, the model presented here can easily be adapted for the grain thinning simulation studies by taking an extra grain boundary transverse direction and thereby having a triad crystalline sample rather than the bicrsytal as used in the present study.

Acknowledgements

The senior author T. O. Ogurtani has the great pleasure to dedicate this paper to his academic advisor and teacher, Emeritus Professor John Shyne of Stanford University, who encouraged him to learn deep insight of many/facets of the kinetics of solid-state phase transformations. The authors also wish to thank Professors William D. Nix of Stanford University, and Dr. Ersin Emre Oren of Washington University, for their very valuable suggestions and encouraging interest in this extensive computational materials science research program at METU. This work is partially supported by the Turkish Scientific and Technical Research Council TUBITAK Grant No. 107M011.

References

Blech, I.A., Kinsborn, E., 1975. Electromigration in thin gold films on molybdenum surfaces. Thin Solid Films 25 (2), 327–334.

Choy, J.-H., Kavanagh, K.L., 2004. Effects of capillary forces on copper/dielectric interfacial void evolution. Applied Physics Letters 84 (25), 5201.

Fischer, A.H., von Glasow, A., Penka, S., Ungar, F., 2002. Electromigration failure mechanism studies on copper interconnects. In: Proceedings of the IEEE International Reliability Physics Symposium, Dallas, pp. 139.

Glickman, E., Nathan, M., 1996. On the unusual electromigration behavior of copper interconnects. Journal of Applied Physics 80 (7), 3782.

He, J., Suo, Z., Marieb, T.N., Maiz, J.A., 2004. Electromigration lifetime and critical void volume. Applied Physics Letters 85 (20), 4639.

Ho, P.S., 1970. Motion of inclusion induced by a direct current and a temperature gradient. Journal of Applied Physics 41 (1), 64.
Hu, C.-K., Lee, K.Y., Gignac, L., Carruthers, R., 1997. Electromigration in 0.25 μm wide Cu line on W. Thin Solid Films 308, 443–447.
Hu, C.-K., Rosenberg, R., Lee, K.Y., 1999. Electromigration path in Cu thin-film lines. Applied Physics Letters 74 (20), 2445–2447.
Hu, C.-K., Gignac, L., Rosenberg, R., Liniger, E., 2001. In: Proceedings of the 1st International Conference on Semiconductor Technology. The Electrochemical Society, Pennington, NJ, 17, pp. 387.
Hu, C.-K., Gignac, L., Rosenberg, R., Liniger, E., Rubino, J., Sambucetti, C., Domenicuci, A., Chen, X., Stamber, A.K., 2002a. Reduced electromigration of Cu wires by surface coating. Applied Physics Letters 81 (10), 1782–1784.
Hu, C.-K., Gignac, L., Rosenberg, R., Liniger, E., Rubino, J., Sambucetti, C., Domenicucci, A., Chen, X., Stamber, A.K., 2002b. Reduced electromigration of Cu wires by surface coating. Applied Physics Letters 81 (10), 1782–1784.
Hu, C.-K, Canaperi, D., Chen, S.T., Gignac, L., Herbst, B., Kaldor, S., Krishnan, M., Liniger, E., Rath, D.L., Restaino, D., Rosenberg, R., Rubino, J., Seo, S.-C., Simon, A., Smith, S., Tseng, W.-T., 2004. In: Proceedings of the IEEE International Reliability Physics Symposium, Phoenix, pp. 222.
Huang, P., Li, Z., Sun, J., 2000. Finite element analysis for surface diffusion-controlled shape instabilities of plate-like grains. Computational Materials Science 20, 66–76.
Khenner, M., Averbuch, A., Israeli, M., Nathan, M., 2001. Numerical simulation of grain-boundary grooving by level set method. Journal of Computational Physics 170 (2), 764–784.
Lee, K.D., Ho, S.P., 2004. Statistical study for electromigration reliability in dual-damascene Cu interconnects. IEEE Transactions on Device and Materials Reliability 4 (2), 237–245.
Liniger, E., Gignac, L., Hu, C.K., Kaldor, S., 2002. In situ study of void growth kinetics in electroplated Cu lines. Journal of Applied Physics 92 (4), 1803–1810.
Lloyd, J.R., Lane, M.W., Liniger, E.G., Hu, C.-K., Shaw, T.M., Rosenberg, R., 2005. Electromigration and adhesion. IEEE Transactions on Device and Materials Reliability 5 (1), 113–118.
Lord Kelvin, W.T., Tait, P.G., 1789. The Elements of Natural Philosophy, second ed. Claredon Press, Oxford.
Mullins, W.W., 1957. Theory of thermal grooving. Journal of Applied Physics 28 (3), 333.
Min, D., Wong, H., 2006. Grain-boundary grooving by surface diffusion with asymmetric and strongly anisotropic surface energies. Journal of Applied Physics 99, 023515.
Nichols, F.A., Mullins, W.W., 1965. Morphological changes of a surface of revolution due to capillarity-induced surface diffusion. Journal of Applied Physics 36 (6), 1826.
Nathan, M., Glickman, E., Khenner, M., Averbuch, A., Israeli, M., 2000. Electromigration drift velocity in Cu interconnects modeled with the level set method. Applied Physics Letters 77 (21), 3355–3357.
Ogurtani, T.O., 1975. The room temperature annealing kinetics of stacking faults in cold worked alpha brasses. Metallurgical Transactions A 6, 493.
Ogurtani, T.O., 2006a. Mesoscopic nonequilibrium thermodynamics of solid surfaces and interfaces with triple junction singularities under the capillary and electromigration forces in anisotropic three-dimensional space. Journal of Chemical Physics 124, 144706.
Ogurtani, T.O., 2006b. Unified theory of linear instability of anisotropic surface and interfaces under capillary, electrostatic, and elastostatic forces: The growth of epitaxial amorphous silicon. Physical Review B 74, 155422–155447.
Ogurtani, T.O., Oren, E.E., 2004. Electromigration-induced void grain-boundary interactions: the mean time to failure for copper interconnects with bamboo and near-bamboo structures. Journal of Applied Physics 96 (12), 7246–7253.
Ogurtani, T.O., Oren, E.E., 2005. Irreversible thermodynamics of triple junctions during the intergranular void motion under the electromigration forces. International Journal of Solids and Structures 42, 3918–3952.
Ogurtani, T.O., Akyildiz, O., 2005. Grain boundary grooving and cathode voiding in bamboo-like metallic interconnects by surface drift diffusion under the capillary and electromigration forces. Journal of Applied Physics 97 (9), 093520.
Ogurtani, T.O., Gungor, M.R., Oren, E.E., 2003. Interactive computer simulation of dislocation damping spectra associated with the coupled motion of geometric kinks and point defects subjected to the bulk segregation phenomenon. Solid State Phenomena 89, 141–190.
Park, C.W., Vook, R.W., 1991. Activation energy for electromigration in Cu films. Applied Physics Letters 59 (2), 175–177.
Park, C.W., Vook, R.W., 1993. Electromigration resistant Cu–Pd alloy films. Thin Solid Films 226 (2), 238–247.
Smithells, C.J., 1967. Metals Reference Book, fourth edition, Butterworths, London, pp. 3, 743.
Tu, K.N., 2003. Recent advances on electromigration in very-large-scale-integration of interconnects. Journal of Applied Physics 94 (9), 5451.
Yeremin, E.N., 1979. The Foundation of Chemical Kinetics. MIR Publishers, Moscow, pp. 215..